analytical chemistry

Article

pubs.acs.org/ac

Collision-Induced Dissociation Ion Mobility Mass Spectrometry for the Elucidation of Unknown Structures in Strained Polycyclic Aromatic Hydrocarbon Macrocycles

Wen Zhang, Martin Quernheim, Hans Joachim Räder,* and Klaus Müllen*

Max Planck Institute for Polymer Research, Ackermannweg 10, D55128 Mainz, Germany

ABSTRACT: Structure determination of unexpected products obtained during synthesis of large carbon nanotube sidewall segments with more than 200 carbon atoms represents a challenging task for traditional analytical methods. Herein, we investigate a homologous series of four products having the same number of carbon atoms but slightly different hydrogen numbers ranging from 168 to 162. We demonstrate that the combination of mass spectrometry, ion mobility separation, and collision-induced dissociation (CID) can be used to finally elucidate the complete structures with high certainty. The postulated 1,2-phenyl shift as origin for the side reaction could be proven by changes in the minimum fragment sizes. A combination of CID and ion mobility spectrometry was applied for the first time to prove the cyclic nature of all molecules by the significant size increase upon ring opening. Thereby, also, more compact molecules were discovered in the gas phase with thus far unknown structures. Finally, the potential presence of numerous isomers could be ruled out by drift time measurements and molecular modeling together with theoretical collision cross-section (CCS) calculations. Surprisingly, only one defined structure could be assigned to each macrocycle in the homologous series, most likely as a result of natural selection rules driven by ring strain and steric hindrance. With a decreasing hydrogen content, the macrocycles undergo a stepwise transition from a cylindrical to conical shape. Overall, ion mobility mass spectrometry together with molecular modeling shows great potential to analyze unknown structures, especially in cases where structure determination by X-ray single-crystal analysis is not applicable.

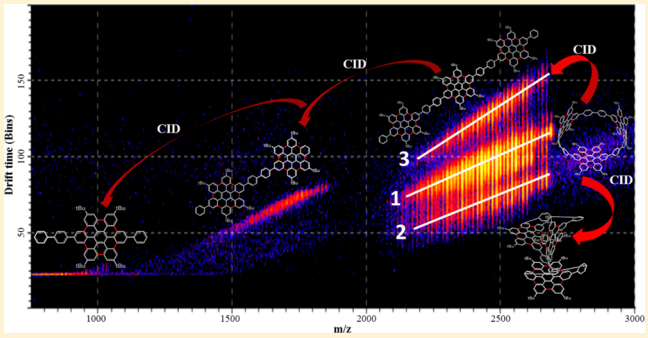

Macrocycles of large polycyclic aromatic hydrocarbons (LPAHs) with the shape of structurally well-defined carbon nanotube (CNT) sidewall segments are model compounds with regard to their chemical, optical, and electronic properties. These macrocycles could be of potential use as seeds for controlled CNT formation with tailored diameters and lattice structures.[1,2] The coveted cyclic ribbon-type, strained structures, however, are challenging for synthesis as well as characterization, especially in the case of unexpected chemical reaction pathways, resulting in unknown structures. For such huge molecular scaffolds with more than 200 carbon atoms, traditional characterization methods, such as nuclear magnetic resonance (NMR), infrared (IR), and ultraviolet (UV) spectroscopy, do not provide sufficient structural information. Thus, there is still a need for additional methods of structure proof.

Herein, we investigate the significance of ion mobility mass spectrometry (MS) for the analysis of intact polycyclic aromatic hydrocarbon (PAH) macrocycle structures and their fragments. In addition to the exact molecular weight information from MS, the combination with ion mobility spectrometry provides supplementary information on the molecular shape.

Scheme 1 illustrates the chemical reaction that gives rise to the present investigation. In a multi-step synthesis, biphenylene-extended cyclic *para*-hexaphenylbenzene macrocycle ([3]CHPB) could be selectively prepared and fully characterized.[3−5] In the final synthesis step, however, where the [3]CHPB unit should be converted into a biphenylene-extended cyclic *para*-hexa-*peri*-benzocoronene macrocycle ([3]CHBC) with 18 new C−C bonds (red color), an unexpected side reaction takes place.

Mass spectrometric analysis of the reaction products revealed that, in addition to the desired product M_0 with the chemical formula $C_{210}H_{168}$, also products with two, four, and six hydrogen atoms less were obtained as the major components, corresponding to the chemical formulas M_2 ($C_{210}H_{166}$), M_4 ($C_{210}H_{164}$), and M_6 ($C_{210}H_{162}$). Hence, neither the structures of the side products nor the nature of the side reaction is known initially. It is also questionable whether these products maintain the cyclic structure.

Whereas MS was the main method to detect the side products, it does not provide information on the molecular shape. Ion mobility spectrometry, as a post-ionization separation method, can separate ions with various sizes, shapes,

Received: October 1, 2015
Accepted: November 27, 2015
Published: November 27, 2015

DOI: 10.1021/acs.analchem.5b03704
Anal. Chem. 2016, 88, 952−959

Scheme 1. Concept of a Selective Dehydrogenation Reaction toward a [3]CHBC Macrocycle with a Cylindrical Shape

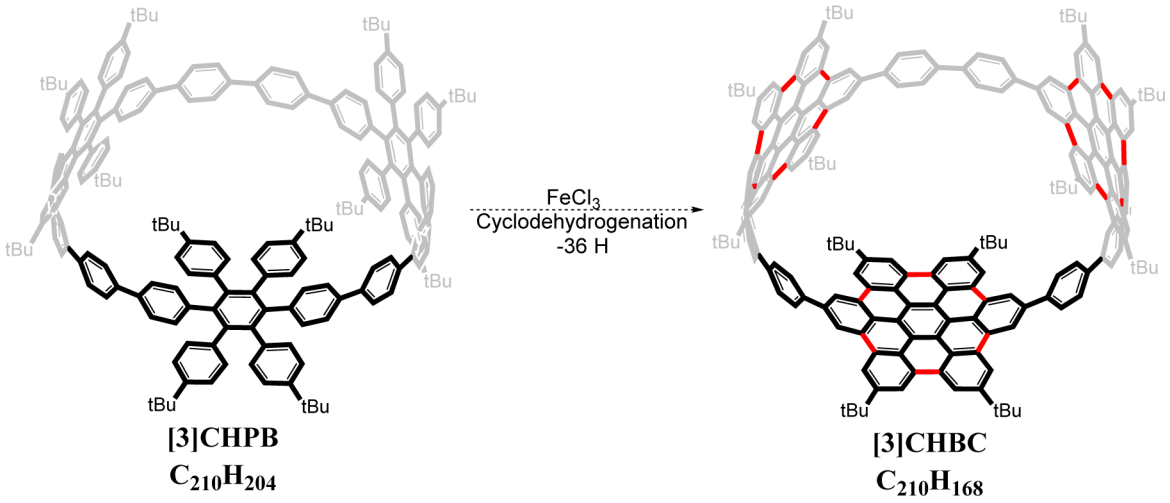

and conformations according to their collision cross-section (CCS), thus representing a complementary method that could also distinguish isomers with the same m/z but different structures.[6,7] Ion mobility mass spectrometry (IMMS) has already been used for the structure and architecture analysis of polymers,[8−14] metallosupramoleculars,[15−20] and biomolecules.[21−25] Hoskins et al.[8] distinguished the linear and cyclic poly(ε-caprolactone) according to their drift time differences in varied charge states by IMMS. Li et al.[15] used IMMS to separate and characterize a series of synthesized linear and cyclic metallosupramoleculars with varied oligomeric numbers. Jia et al.[21] observed the conversion process of peptide sequence scrambling from a linear precursor ion into another rearranged linear ion via an ion cyclization intermediate in the gas phase by IMMS.

Moreover, the linear and cyclic architectures also generate obvious fragmentation pattern differences. Yol et al.[26] investigated the fragmentation patterns of linear and cyclic polystyrenes and polybutadienes by matrix-assisted laser desorption/ionization (MALDI) tandem MS. The results showed substantially different fragment ion distributions. Wesdemiotis et al.[13,14] reviewed the structure characterization of cyclic polymers by multidimensional MS methods and recommended a combination of ion mobility separation with tandem MS for the analysis approach of particularly difficult cases. However, the potential of IMMS for structure elucidation of unknown molecules, such as our rigid and complex LPAHs, has not yet been addressed.

In the present paper, we make use of IMMS for the characterization of our LPAH macrocycles in general and elucidate its ability to analyze unknown structure changes in particular. In addition to the investigation of intact macrocycles, we especially explore their fragmentation behavior by a combination of precursor ion selection with collision-induced dissociation (CID) and ion mobility spectrometry to analyze the molecular shape of the LPAH macrocycle fragments.

EXPERIMENTAL SECTION

Synthesis and Purification. The bottom-up synthesis and purification of the LPAH macrocycles were described in our previous work.[3−5] The [3]CHPB macrocycle could be effectively prepared via multi-step routing. The final step to synthesize the biphenyl-extended cyclo-hexa-*peri*-benzocorenene trimer [3]CHBC included the oxidative cyclodehydrogenation of the biphenylene-extended cyclo-hexaphenylbenzene trimer ([3]CHPB) with $FeCl_3$ (Scheme 1). Therefore, [3]CHPB (0.01 g, 0.0037 mmol) was dissolved in unstabilized dichloromethane (10 mL), and a solution of iron(III) chloride (0.086 g, 0.53 mmol) in nitromethane (2 mL) was added at room temperature. The solution was stirred at room temperature for 7 h, while argon was bubbled continuously through the mixture. After quenching with methanol, the mixture was extracted with dichloromethane. The organic layers were separated, washed with brine, and dried over $MgSO_4$. Initially, the raw product was purified by column chromatography on silica (dichloromethane as an eluent). Furthermore, the product mixture was separated by preparative high-performance liquid chromatography (HPLC) with a HPLC facility from Shimadzu, series CBM 20A, a pump LC-20AD, and a SPD-20A UV−vis detector (λ = 320 nm), using the column Cosmosil 5PBB (inner diameter of 10 × 250 mm) from Nacalai Tesque. A toluene/MeOH mixture (from 3:1 to 9:1) was used as an eluent to isolate the four major product fractions.

MALDI IMMS. All MS experiments were performed on a SYNAPT G2-Si instrument (Waters Corp., Manchester, U.K.) equipped with a MALDI source. {(2*E*)-2-Methyl-3-[4-(2-methyl-2-propanyl)phenyl]-2-propen-1-ylidene}malononitrile (DCTB) was used as the matrix for MALDI MS measurement. The mass and ion mobility data analyses were performed on Masslynx V4.1 and Driftscope V2.8, respectively. Ion mobility mass spectrometry (HDMS mode), ion mobility tandem mass spectrometry (HDMS/MS mode), and tandem mass spectrometry (MS/MS mode) were employed for analysis of the LPAHs. A high trap direct current (DC) bias value of 120 V was used in all of the experiments to support the transmission of high mass ions.

Ion Mobility Mass Spectrometry (HDMS Mode). Mass spectra were acquired in positive-ion mode over the mass range of 50−3000 Da. Helium cell gas flow was set at 180 mL min^{-1}, and IMS gas flow (N_2) was set at 80 mL min^{-1}. The IMS was operated with 40 V wave height and 180 m s^{-1} wave velocity.

Ion Mobility Tandem Mass Spectrometry (HDMSMS Mode). Besides using the above settings in HDMS mode, an increasing collision energy of 0, 100, 150, and 200 V was applied successively in the trap cell before IMS separation. The precursor selection for ions of the four dehydrogenation

DOI: 10.1021/acs.analchem.5b03704
Anal. Chem. 2016, 88, 952−959

products was performed at masses of 2691, 2689, 2687, and 2685 Da with a selection window of approximately 1 Da.

Tandem Mass Spectrometry (MS/MS Mode). After selection of the precursor ions, the maximal collision energy of 200 V was applied in the trap cell for each dehydrogenation product. The monomeric fragments were recorded with a mass range of 300−1200 Da.

CCS Value Calculation. The chemical structures were energy-optimized by the open source Avogadro software[27] V2 0.7.2 at the MMFF94 level of theory. The CCS values were then calculated by Driftscope CCS calculation software (V2.8, Waters Corp., Manchester, U.K.).

RESULTS AND DISCUSSION

Measurement of Intact LPAH in IMMS. The primary question about the structure of the unexpected dehydrogenation products is whether these molecules have a comparable shape and if they are still macrocycles or not. Therefore, the product mixture was first separated by preparative HPLC. The individual fractions of the homologous series of products M_0 ($C_{210}H_{168}$), M_2 ($C_{210}H_{166}$), M_4 ($C_{210}H_{164}$), and M_6 ($C_{210}H_{162}$) were then ionized by MALDI and submitted to ion mobility measurements to gain first insights into molecular shape differences.

To eliminate the drift time differences resulting from the slightly different molecular weights of the four samples, only one isotope of each molecule at the same nominal mass was selected for comparison. Therefore, the ion mobility spectra of M_0, M_2, M_4, and M_6 molecules at the isotopic mass of 2689 Da, which is present in all four isotopic distributions, were extracted in Figure 1.

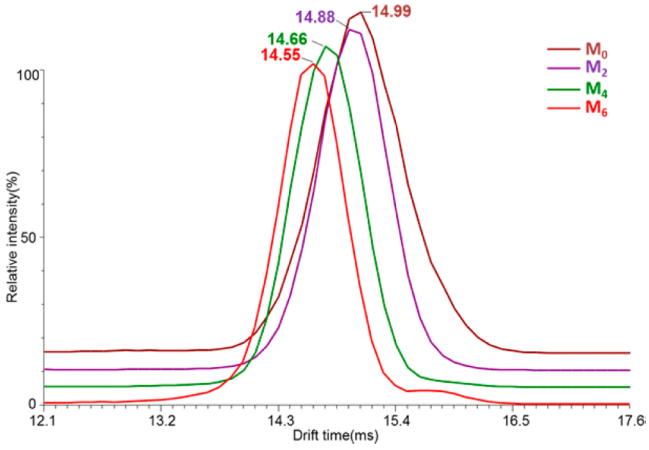

Figure 1. Ion mobility analysis of M_0, M_2, M_4, and M_6 product molecular ions.

As a result, the ion mobility measurements show only one peak for each molecular ion with only small differences in drift time and peak maxima among M_0, M_2, M_4, and M_6. According to Mason−Schamp equation,[28,29] when using the same experimental parameters, the drift time differences mainly arise from the differences in the molecular size and m/z. Using the same m/z for the different samples, this drift time difference clearly indicates that the molecules are becoming slightly smaller with an increasing degree of overdehydrogenation within the four product molecules. In addition, the peak width shrinks clearly from 1.00 to 0.77 ms at half peak height in the same order.

Measurement of LPAH Fragments in IMMS. For additional structural information, we submitted the homologous series of LPAHs to CID measurements and investigated the fragments and their drift time spectra at increasing collision energies up to 200 V.

Therefore, the molecular ion of each dehydrogenated product was selected as the parent ion in ion mobility tandem MS experiments. On the whole, the four reaction products M_0, M_2, M_4, and M_6 generated similar fragmentation patterns in IMMS. As representative for all measurements, Figure 2 shows

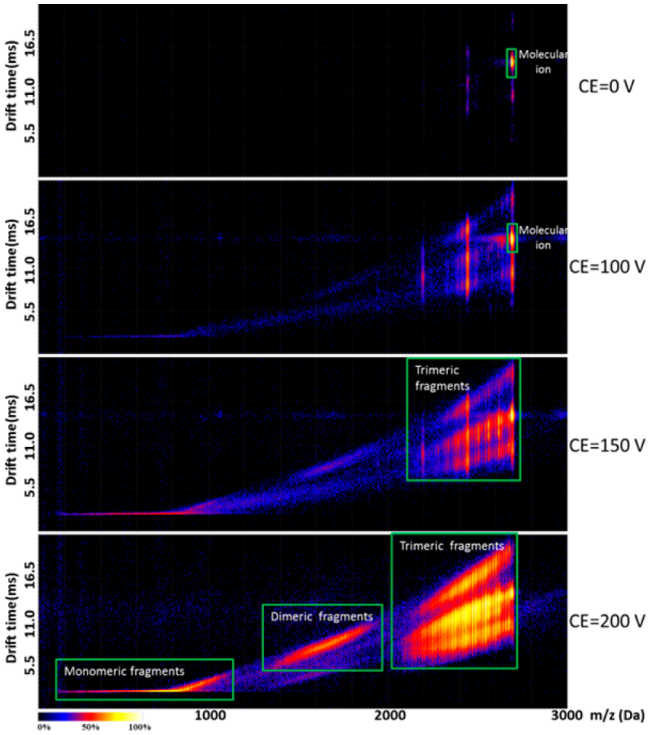

Figure 2. Two-dimensional drift time versus m/z ion mobility image with increasing collision energy for sample M_4.

the two-dimensional (2D) drift time versus m/z spectra of M_4 at collision energies of 0, 100, 150, and 200 V. A higher brightness of the color indicates a higher peak intensity.

Up to the collision energy of 100 V, mainly the peak of the intact LPAH molecule is present. A few signals with intensities lower than 1% of that of the molecular ion come from slight fragmentation of the precursor ions. Significant fragmentation starts at a collision energy of 150 V. When the collision energy is further increased to the maximum of 200 V, three groups of fragments at different mass ranges were produced. With regard to the desired macrocycle, which consists of three hexa-*peri*-benzocoronene (HBC) units connected by three biphenyl bridges, the three molecular weight regions can be assigned to fragments including one, two, and three HBC units (mono-, di-, and trimeric fragment ions).

Figure 3 depicts the magnified 2D drift time versus m/z ion mobility image for sample M_6 at 200 V collision energy. The close similarity in comparison to the 200 V fragmentation pattern of M_4 in Figure 2 is quite obvious.

Beyond the different mass regions for mono-, di-, and trimeric fragments, Figure 3 also shows a splitting within the trimeric fragment region into three different trend lines. Generally, the series of signals within the trend lines can be

DOI: 10.1021/acs.analchem.5b03704
Anal. Chem. 2016, 88, 952−959

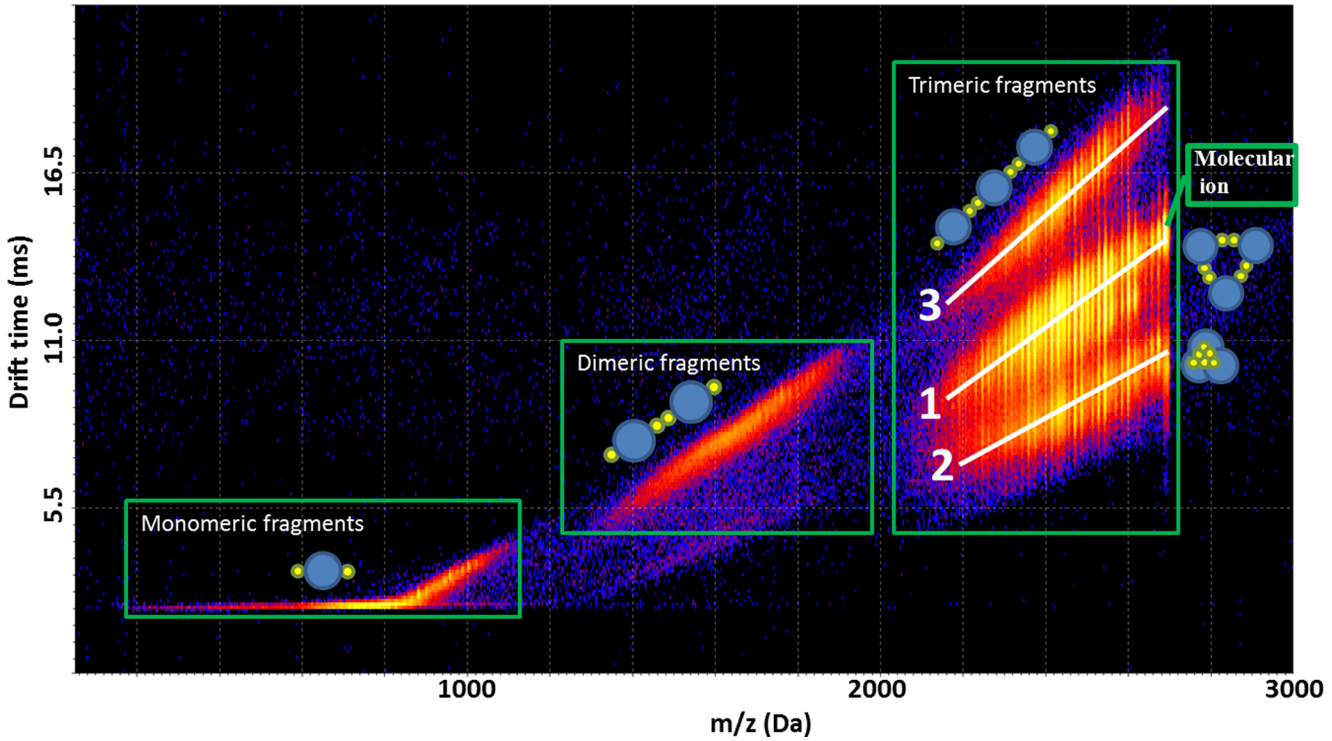

Figure 3. Magnified 2D drift time versus m/z mobility image for sample M_6.

attributed to a consecutive loss of alkyl groups, originating from the 12 *tert*-butyl substituents attached to the HBC units.

The existence of the trend lines indicates that there are three different initial structures with significant different molecular sizes, from which the alkyl groups are released. The three trend lines were numbered to indicate the sequence of appearance with increasing collision energy. Trend line 1 is already present at low collision energies, and also the intact molecular ion belongs to it. Then, trend line 2 appears at increased collision energy. Finally, trend line 3 appears at maximum collision energy, while mono- and dimeric fragments are observed too.

From the fact that the intact molecular ion measured without collision energy belongs to trend line 1, we conclude that the alkyl group loss within this series originates from intact macrocyclic structures.

Ions in trend line 3 have significantly higher drift times than those in trend line 1 and, thus, belong to bigger structures with higher CCS. This trend line shows high intensity at the highest collision energies, and we assign it to the ring-opened structures. Therefore, one break inside the cyclic framework is required, and the consecutive alkyl group loss takes place from linear structures. The di- and monomeric fragments, which also appear at the highest collision energies, own two breaks within the cyclic framework. They only show one trend line, indicating only one general shape of the residual mainframe, where the consecutive loss of side chains takes place. This is quite comprehensible because the macrocycle backbone is a rigid rod structure as soon as ring opening takes place.

Astonishingly and unexpectedly, a further trend line is observed already being present at intermediate collision energies. This trend line originates from structures having a significantly smaller CCS and, thus, a smaller size than the macrocycle itself. It is quite remarkable to detect smaller structures than the desired macrocycle, because it already consists of 15 phenyl rings connected in *para* positions, a framework that tends to be a linear rigid rod but is bent to a cyclus with high ring strain. To date, we can only speculate about this very compact structure, and it is an object of ongoing investigations. The fragmentation pattern observed here provides a novel approach to distinguish the cyclic structure from its linear counterpart, and this method may also be useful for the characterization of other macrocycles by MS.

The structural assignment of the trimeric fragments can be supported by theoretical calculations of CCS for the cyclic and ring-opened structures. In the case of our LPAH molecules, the calculated CCS values for cyclic and linear architectures of M_0 molecules possess significantly different values of 636.94 and 831.24 Å^2, respectively. The ring-opening reaction in the gas phase, thus, considerably increases the CCS value, especially in the case of our structures, which own a linear rigid paraphenylene backbone.[30] Our results correlate well with the relative CCS value differences observed for cyclic and linear metallosupramolecular assemblies of Zn^{II} ions and bis-(terpyridin) ligands reported by Wesdemiotis and co-workers.[14,15]

Because of the fact that all molecules of the investigated series herein [M_0, ($C_{210}H_{168}$), M_2 ($C_{210}H_{166}$), M_4 ($C_{210}H_{164}$), and M_6 ($C_{210}H_{162}$)] show the same general behavior, we can conclude that the initially targeted molecule M_0 as well as the thus far unknown side products M_2, M_4, and M_6 all own a cyclic framework.

Structural Elucidation from Monomeric Fragments. After identification of the cyclic nature of the intact four dehydrogenated product molecules, the next question is to figure out the structure of the macrocyclic building blocks. Because there is additional hydrogen loss while the hexaphenylbenzene (HPB) monomer in the macrocycles is already fully condensed, there is still a need for elucidation of the origin of the side reactions. A possible explanation for the

DOI: 10.1021/acs.analchem.5b03704
Anal. Chem. 2016, 88, 952−959

extra mass loss of two, four, and six hydrogens could be a rearrangement reaction during cyclodehydrogenation in the final step of synthesis. A rearrangement reaction by a 1,2-phenyl shift at the main PAH framework was previously already observed as a side reaction in our group.[31] In the case of our strained LPAH macrocycles, we rationalize that this type of unexpected rearrangement reaction could be even more pronounced because of the release of ring stain. With each 1,2-phenyl shift, the macrocyclic framework gains preformed 60° angles as opposed to the initially linear but bent paraphenylene connection. Therefore, the macrocyclic system loses potential energy with each rearrangement reaction. Because each rearrangement reaction is equivalent with an additional loss of two hydrogen atoms, we could expect up to three rearrangement reactions in our series M_2, M_4, and M_6. Thus far, measurements by nuclear magnetic resonance (NMR) support this theory;[4,5] however, in a framework with more than 200 carbon atoms, it is not a sufficient structure proof for such postulated 1,2-phenyl shift reactions in the macrocycles. In addition, the 1,2-phenyl shift side reactions could give rise to numerous isomers. In the case of two or more rearrangement reactions, the condensed cores of M_4 and M_6 could theoretically include one or two side reactions within one core unit, as illustrated in Figure 4. Figure 4 also visualizes all possible individual core structures, which could be constituents in macrocycles with one, two, or more side reactions in general.

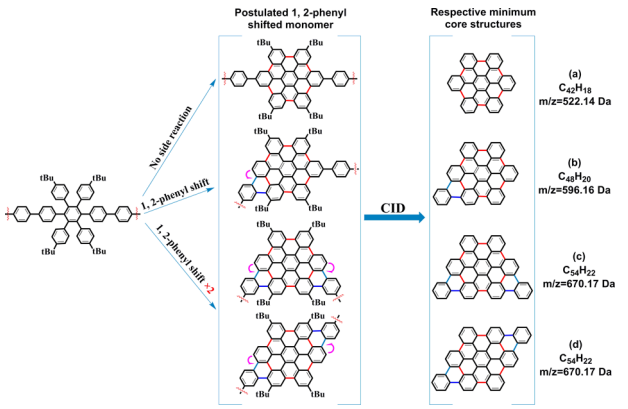

Figure 4. All possible monomeric structures after 1,2-phenyl shift reactions and respective inner core structures inside the LPAH macrocycles.

For this reason, we investigate the regions of the monomeric fragments in more detail. Assuming that the fully condensed core units in Figure 4 represent very stable fragments, which should represent the minimum fragment size after the loss of single bonded alkyl groups and phenylene bridges, we should gain the minimum core size information from the different minimum fragment sizes in the monomeric region in the mass spectrum.

Therefore, tandem MS was applied, and the precursor ions at m/z 2691 Da (M_0), 2689 Da (M_2), 2687 Da (M_4), and 2685 Da (M_6) were selected for fragmentation. Parameters were optimized to enhance the monomeric fragment intensity while the maximal 200 V collision energy was applied. The MS/MS spectra of monomeric fragments of the four samples were illustrated in Figure 5.

For the M_6 macrocycle, the mass range of monomeric fragments is relatively narrow and there is no signal in the mass range lower than m/z 596 Da (indicated by an arrow in Figure 5). This mass value fits to the minimum core size with one 1,2-phenyl shift, as illustrated in Figure 4b. Hence, it can be concluded that the three 1,2-phenyl shifts within the macrocycle are distributed over three core units, with one phenyl shift in each constituting unit, and that no HBC cores are present in the precursor macrocycle M_6. Otherwise, in the case of at least one HBC monomer without 1,2-phenyl shift reaction, the HBC core (m/z 522 Da) should be present as the minimum fragment size, as observed in M_0, M_2, and M_4. Because the rearrangement happens only once in each core unit, the theoretical core units with two rearrangements within one unit, as illustrated in panels c and d of Figure 4, seem to be less favorable.

As expected for the targeted macrocycle M_0, the fragment signals at the low mass side end at m/z 522 Da, confirming the HBC cores (Figure 4a) as the constitutive units. Consequently, the fragmentation patterns of M_2 and M_4 should include fragments with 596 and 522 Da with regard to the minimum fragment core sizes of Figure 4, which can be confirmed too. Therefore, these M_2 and M_4 macrocycles should consist of one and two 1,2-phenyl-shifted core units connected by two and one biphenylene bridges, respectively.

Comprehensive Structure Elucidation. The final question about the macrocycle structure is the sequence of the monomer building blocks inside the macrocycles.

According to the fragmentation patterns above, we know that M_6 consists of three 1,2-phenyl-shifted core units. Thus, M_4 consists of two rearranged HBC units, and M_2 consists of one rearranged HBC unit. Finally, the initially targeted M_0 macrocycle consists of three unchanged HBC monomers. While there could be only one isomer for the macrocycles M_0 and M_2, the macrocycles M_4 and M_6 could theoretically be a mixture of isomers resulting from the different positions of the rearranged molecule parts toward each other. Inside the cyclus, two rearranged HBC cores could be oriented in three ways: head to tail, head to head, or tail to tail. Thus, the three PAH constituents in M_4 could be either connected by two phenylene bridges and one biphenylene bridge (panels a and c of Figure 6) or by one single bond and two biphenyl bridges (Figure 6b). Analogously, the three constituents in M_6 could be connected by three phenylene bridges (Figure 6d) or, alternatively, by one single bond, one phenylene bridge, and one biphenylene bridge (Figure 6e).

Conclusions from Ion Mobility Measurements. As previously shown in Figure 1, the ion mobility signals of the molecular ions of the four dehydrogenated products show very similar drift times, shifting with small increments successively to lower values with increasing hydrogen loss of the macrocycles. Also, the peak widths shrink in the same direction. Hence, there is no direct evidence for the existence of isomers, or if isomers should exist, they must have the same CCS value.

The decrease in the drift time with an increasing number of rearrangement reactions from M_0 to M_6 implies that the introduction of each rearranged HBC unit leads to a small but measurable shrink of the molecular size.

Conclusions from Three-Dimensional (3D) Structure Simulations. To obtain further information on the existence of isomers, we prepared 3D structure simulations with corresponding CCS value calculations for M_0, M_2, and all potential isomers for M_4 and M_6. The obtained CCS values are summarized in Table 1.

DOI: 10.1021/acs.analchem.5b03704
Anal. Chem. 2016, 88, 952−959

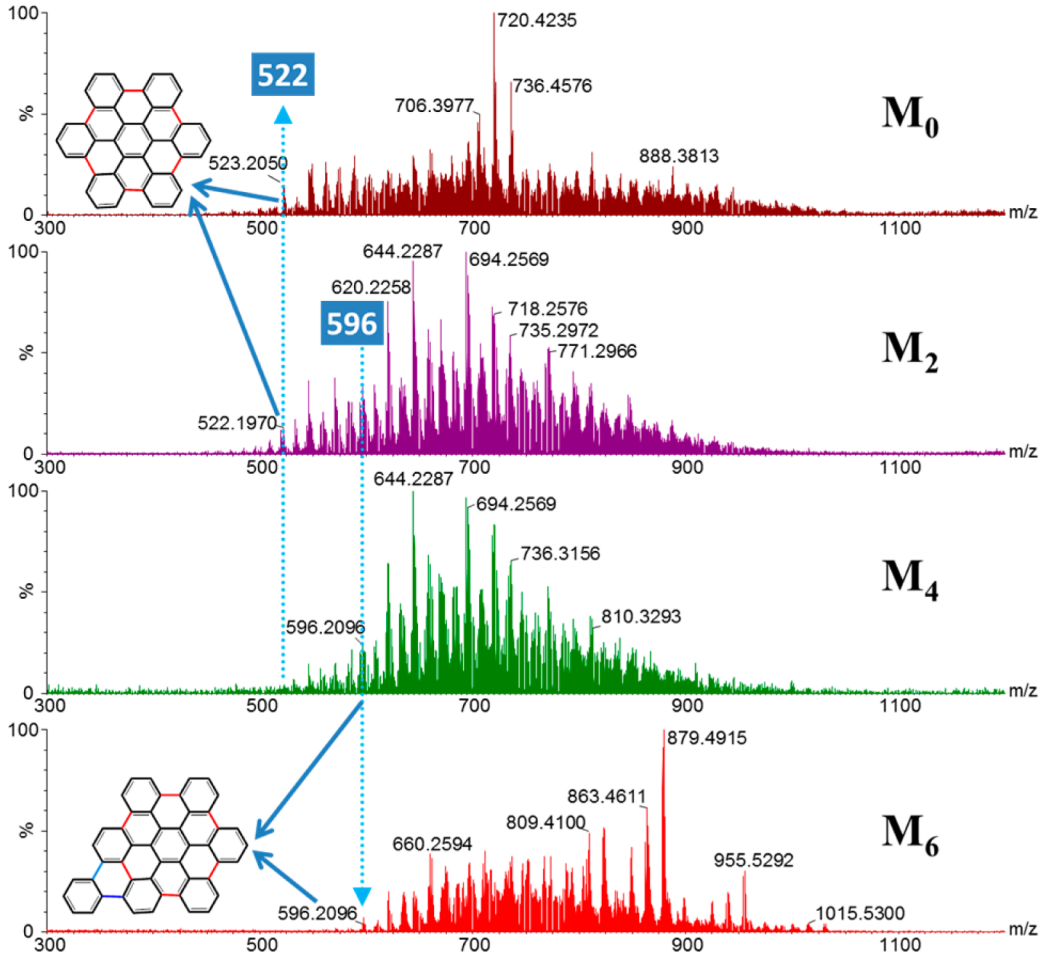

Figure 5. MS/MS spectra of monomeric fragments of M_0, M_2, M_4, and M_6 macrocycles.

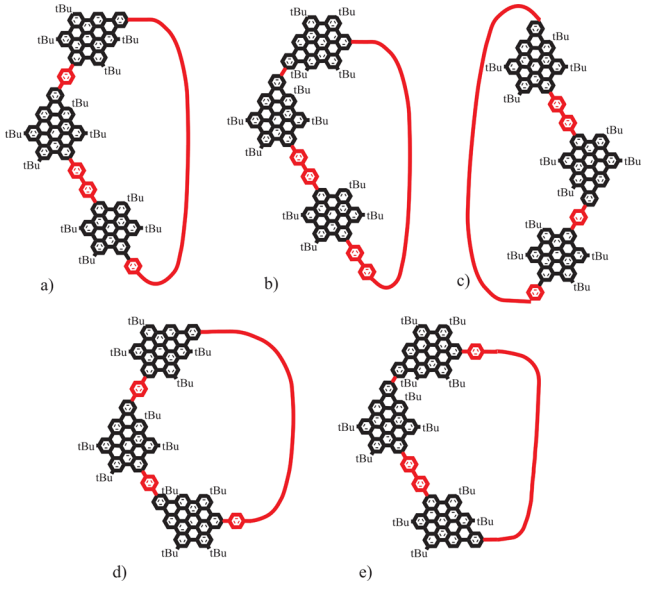

Figure 6. Potential isomers of M_4 and M_6 with regard to the rearrangement positions within the macrocycles. The bridging units are marked in red. (a) M_4, head to tail connection; (b) M_4, head to head connection; (c) M_4, tail to tail connection; (d) M_6, head to tail connection of all units; and (e) M_6, one head to head, one head to tail, and one tail to tail connection.

Table 1. Calculated CCS Values for the Most Representative Isomers of Macrocycles M_0–M_6

	isomer 1 (Å^2)	isomer 2 (Å^2)	isomer 3 (Å^2)
M_0	636.96		
M_2	631.79		
M_4	625.65 (Figure 6a)	655.90 (Figure 6b)	657.06 (Figure 6c)
M_6	619.74 (Figure 6d)	645.10 (Figure 6e)	

From the comparison of CCS values calculated for isomers of M_4, it is obvious that the head to head connected structure (Figure 6b) and tail to tail connected structure (Figure 6c) have significantly higher values in comparison to the head to tail connected isomer (Figure 6a). The same holds true for the head to head connected isomer of M_6. The existence of both isomers in a mixture should therefore cause at least a significant peak broadening in the drift time signals of M_4 and M_6, which is experimentally not the case (see Figure 1). If we further compare the CCS values of M_0, M_2, and the head to tail connected isomers of M_4 and M_6, we find a small but continuously shrinking size of the macrocycles, which reproduces exactly the observed experimental behavior in the drift time measurements.

Thus, it is surprisingly clear at this point that one can exclude the presence of head to head connected isomers in all cases and the structures of the four different macrocycles can be

DOI: 10.1021/acs.analchem.5b03704
Anal. Chem. 2016, 88, 952–959

visualized with high certainty, as presented in Figure 7. It is quite remarkable that only one isomer of each molecule is left

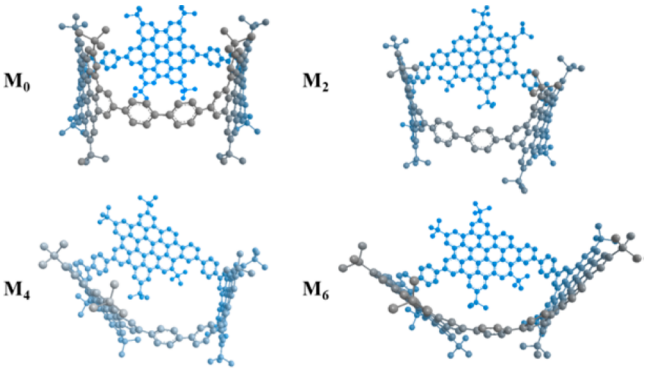

Figure 7. Ball-and-stick models of four macrocycle products.

as the most probable structure from all possible isomers, which could be formed theoretically. We attribute this to a "natural selection" driven by ring strain and steric hindrance.

The macrocycles undergo a successive transition from a cylindrical shape in the case of M_0 to a conical shape in the case of M_6. From these architectures, one could also justify the relative high drift time peak width of M_0 compared to the other macrocycles. Because of the high conformational flexibility, the HBC cores in M_0 might be able to oscillate or rotate within the cyclic framework. This tendency is reduced in the order M_2, M_4, and M_6, because the successive introduction of rearranged core units introduces each a 60° angle, thereby decreasing the probability for core rotations within the cyclic framework.

CONCLUSION

The combination of MS, collision-induced fragmentation, and ion mobility measurements was employed to elucidate initially unknown structures obtained as unexpected main products during the final step of a LPAH macrocycle synthesis.

Taken as a whole, all results of the present work confirm the postulated 1,2-phenyl shift as a side reaction, which happens up to 3 times during cyclodehydrogenation toward the fully condensed PAH units. The unusual high tendency for 1,2-phenyl shift reactions inside the cycle is plausible because of the release of ring strain by introducing 60° angles with each phenyl shift in a cyclic lattice that tends to be linear.

From the numerous possible isomers that could be produced in the case of two and three 1,2-phenyl shifts within one molecule, remarkably, only one isomer in each case is left as the most probable structure. This can be concluded from the minimum core size information obtained from CID fragmentation, the measurement of drift times, and the comparison to 3D molecular structure simulations.

The structures of the four reaction products can thus be provided with high certainty, as visualized in Figure 7. Even in the case of M_4 and M_6, where different connections of the core subunits from single bonds over phenylenes to biphenylenes could be present, the CCS values from simulations allow for the exclusion of the existence of isomers other than such with head to tail connection. This astonishing finding is most likely due to "natural" selection rules, driven by ring strain and steric hindrance during the chemical reaction.

Besides the structure elucidation for our specific molecules, the herein applied methodology could also be of more general use for analytics of macrocycles. The combination of CID excitation and subsequent ion mobility investigation of the fragments shows ring opening and, thus, allows for proving the cyclic nature of complex molecules where traditional methods fail.

Beyond ring opening, which produces significantly less compact structures compared to the cycles, another interesting phenomenon within the homologous series M_0, M_2, M_4, and M_6 is the appearance of significantly more compact structures upon CID excitation. This is quite remarkable, because the macrocycles themselves are already strained systems, which try to relax by 1,2-phenyl shifts during synthesis. The nature of the compact structures is thus far unknown but will be the object of further investigations.

Overall, the results demonstrate that the combination of MS, ion mobility, and molecular modeling has great potential for structure elucidation, especially in the case of complex molecules, where NMR spectroscopy fails to give reliable results and where single-crystal X-ray analysis cannot be obtained.

AUTHOR INFORMATION

Corresponding Authors

*E-mail: raeder@mpip-mainz.mpg.de.
*E-mail: muellen@mpip-mainz.mpg.de.

Notes

The authors declare no competing financial interest.

ACKNOWLEDGMENTS

The authors acknowledge financial support from the European Research Council (ERC) Advanced Grant 267160 (NANOGRAPH) and Graphene Flagship (CNECT-ICT-604391).

REFERENCES

(1) Jasti, R.; Bertozzi, C. R. *Chem. Phys. Lett.* **2010**, *494*, 1.
(2) Omachi, H.; Nakayama, T.; Takahashi, E.; Segawa, Y.; Itami, K. *Nat. Chem.* **2013**, *5*, 572.
(3) Nishiuchi, T.; Feng, X.; Enkelmann, V.; Wagner, M.; Müllen, K. *Chem. - Eur. J.* **2012**, *18*, 16621.
(4) Golling, F. E.; Quernheim, M.; Wagner, M.; Nishiuchi, T.; Müllen, K. *Angew. Chem., Int. Ed.* **2014**, *53*, 1525.
(5) Quernheim, M.; Golling, F. E.; Zhang, W.; Wagner, M.; Rader, H.-J.; Nishiuchi, T.; Mullen, K. *Angew. Chem., Int. Ed.* **2015**, *54*, 10341.
(6) Kanu, A. B.; Dwivedi, P.; Tam, M.; Matz, L.; Hill, H. H. *J. Mass Spectrom.* **2008**, *43*, 1.
(7) Mukhopadhyay, R. *Anal. Chem.* **2008**, *80*, 7918.
(8) Hoskins, J. N.; Trimpin, S.; Grayson, S. M. *Macromolecules* **2011**, *44*, 6915.
(9) Song, J. K.; Grun, C. H.; Heeren, R. M. A.; Janssen, H. G.; van den Brink, O. F. *Angew. Chem., Int. Ed.* **2010**, *49*, 10168.
(10) Trimpin, S.; Plasencia, M.; Isailovic, D.; Clemmer, D. E. *Anal. Chem.* **2007**, *79*, 7965.
(11) Trimpin, S.; Clemmer, D. E. *Anal. Chem.* **2008**, *80*, 9073.
(12) Barrere, C.; Selmi, W.; Hubert-Roux, M.; Coupin, T.; Assumani, B.; Afonso, C.; Giusti, P. *Polym. Chem.* **2014**, *5*, 3576.
(13) Li, X. P.; Guo, L.; Casiano-Maldonado, M.; Zhang, D. H.; Wesdemiotis, C. *Macromolecules* **2011**, *44*, 4555.
(14) Yol, A. M.; Wesdemiotis, C. *React. Funct. Polym.* **2014**, *80*, 95.
(15) Li, X. P.; Chan, Y. T.; Casiano-Maldonado, M.; Yu, J.; Carri, G. A.; Newkome, G. R.; Wesdemiotis, C. *Anal. Chem.* **2011**, *83*, 6667.
(16) Chan, Y. T.; Li, X. P.; Yu, J.; Carri, G. A.; Moorefield, C. N.; Newkome, G. R.; Wesdemiotis, C. *J. Am. Chem. Soc.* **2011**, *133*, 11967.
(17) Li, X.; Chan, Y. T.; Newkome, G. R.; Wesdemiotis, C. *Anal. Chem.* **2011**, *83*, 1284.

DOI: 10.1021/acs.analchem.5b03704
Anal. Chem. 2016, 88, 952−959

(18) Schultz, A.; Li, X. P.; Moorefield, C. N.; Wesdemiotis, C.; Newkome, G. R. *Eur. J. Inorg. Chem.* **2013**, *2013*, 2492.
(19) Chan, Y. T.; Li, X. P.; Soler, M.; Wang, J. L.; Wesdemiotis, C.; Newkome, G. R. *J. Am. Chem. Soc.* **2009**, *131*, 16395.
(20) Schultz, A.; Li, X. P.; Barkakaty, B.; Moorefield, C. N.; Wesdemiotis, C.; Newkome, G. R. *J. Am. Chem. Soc.* **2012**, *134*, 7672.
(21) Jia, C. X.; Wu, Z.; Lietz, C. B.; Liang, Z. D.; Cui, Q.; Li, L. J. *Anal. Chem.* **2014**, *86*, 2917.
(22) Ruotolo, B. T.; Benesch, J. L. P.; Sandercock, A. M.; Hyung, S. J.; Robinson, C. V. *Nat. Protoc.* **2008**, *3*, 1139.
(23) Zhou, M.; Politis, A.; Davies, R. B.; Liko, I.; Wu, K. J.; Stewart, A. G.; Stock, D.; Robinson, C. V. *Nat. Chem.* **2014**, *6*, 208.
(24) Polfer, N. C.; Bohrer, B. C.; Plasencia, M. D.; Paizs, B.; Clemmer, D. E. *J. Phys. Chem. A* **2008**, *112*, 1286.
(25) Sabareesh, V.; Manikandan, K.; Sinha, K. M. *Int. J. Mass Spectrom.* **2014**, *364*, 9.
(26) Yol, A. M.; Dabney, D.; Wang, S. F.; Laurent, B. A.; Foster, M. D.; Quirk, R. P.; Grayson, S. M.; Wesdemiotis, C. *J. Am. Soc. Mass Spectrom.* **2013**, *24*, 74.
(27) Hanwell, M. D.; Curtis, D. E.; Lonie, D. C.; Vandermeersch, T.; Zurek, E.; Hutchison, G. R. *J. Cheminf.* **2012**, *4*, 17.
(28) Ahmed, A.; Cho, Y. J.; No, M. H.; Koh, J.; Tomczyk, N.; Giles, K.; Yoo, J. S.; Kim, S. *Anal. Chem.* **2011**, *83*, 77.
(29) Smith, D. P.; Knapman, T. W.; Campuzano, I.; Malham, R. W.; Berryman, J. T.; Radford, S. E.; Ashcroft, A. E. *Eur. Mass Spectrom.* **2009**, *15*, 113.
(30) Fasciotti, M.; Lalli, P.; Heerdt, G.; Steffen, R.; Corilo, Y.; de Sá, G.; Daroda, R.; Reis, F. M.; Morgon, N.; Pereira, R. L.; Eberlin, M.; Klitzke, C. *Int. J. Ion Mobility Spectrom.* **2013**, *16*, 117.
(31) Yoshimura, K.; Przybilla, L.; Ito, S. J.; Brand, J. D.; Wehmeir, M.; Rader, H. J.; Mullen, K. *Macromol. Chem. Phys.* **2001**, *202*, 215.

DOI: 10.1021/acs.analchem.5b03704
Anal. Chem. 2016, 88, 952−959